CONF-821155--5

INTERNATIONAL MEETING ON RESEARCH AND

TEST REACTOR CORE CONVERSIONS FROM

HEU TO LEU FUELS

CONF-821155--5

DE83 007726

Argonne National Laboratory

November 8-10, 1982

NEUTRONICS ANALYSIS OF THE PROPOSED 25-MW LEU TRIGA MULTIPURPOSE RESEARCH REACTOR*

Martias Nurdin

Research Centre for Nuclear Techniques
National Atomic Energy Agency
Republic of Indonesia

and

M. M. Bretscher and J. L. Snelgrove

Argonne National Laboratory
United States of America

*Work performed under the auspices of the U.S. Department of Energy and the International Atomic Energy Agency.

1. INTRODUCTION

More than two years ago the government of Indonesia announced plans to purchase a research reactor for the Puspiptek Research Center in Serpong, Indonesia to be used for isotope production, materials testing, neutron physics measurements, and reactor operator training. Reactors using low-enriched uranium (LEU) plate-type and rod-type fuel elements were considered. This paper deals with the neutronic evaluation of the rod-type 25-MW LEU TRIGA Multipurpose Research Reactor (MPRR) proposed by the General Atomic Company of the United States of America.[1]

2. REACTOR AND FUEL ELEMENT DESCRIPTIONS

The 25-MW TRIGA Multipurpose Research Reactor is of the swimming pool type and is fueled by U-ZrH-Er rods arranged in 36-rod clusters or fuel elements. The core, which has an active height of 22 in., is water-moderated and beryllium-reflected.

An 11 x 12 aluminum grid plate is used to position the nominal core consisting of 40 fuel elements, a central 14.7-cm-square cavity and six 7.34-cm-square in-core irradiation positions. The active core is surrounded by 50 beryllium reflector blocks, half of which contain central irradiation holes. Six natural boron carbide rods are used to control the reactor. Figure 1 shows the arrangement of the fuel, control, irradiation, and beryllium reflector elements. Not shown in the figure are three eight-inch-diameter radial beam tubes and one through tube tangent to the core at the lower flat face. Normally the in-core irradiation spaces would contain experiments or dummy experiments to reduce, for safety reasons, power peaking in adjacent fuel rods. For calculational purposes, however, these in-core irradiation positions were assumed to be water-filled.

The fuel elements consist of 36 fuel rods arranged in a 6 x 6 square array within a square aluminum shroud 7.34 cm on a side. Table 1 describes the fuel pins, which are clad in Incoloy 800, and the 36-rod fuel cluster.

3. CALCULATIONAL METHODS

The calculational methods used in this study are those which have been described in detail in Appendix A of Ref. 2. A brief description of these basic methods is given below.

The EPRI-CELL code[3] was used to generate broad group, burnup-dependent cross sections and atom densities for subsequent diffusion-theory and transport-theory calculations. EPRI-CELL combines a GAM-1[4] resonance treatment in the epithermal energy range with a THERMOS[5] heterogeneous, integral-transport treatment in the thermal energy range. As input, EPRI-CELL utilizes a 68-group epithermal GAM library updated with ENDF/B-IV data processed using the integral-transport option of the MC^2-2[6] code to account for resonance self-shielding and a 35-group thermal THERMOS library updated with ENDF/B-IV data processed using either the XLACS1 module of the AMPX system[7] or the NJOY code.[8] Spatial self-shielding factors, calculated using MC^2-2, were also used as input to EPRI-CELL.

The MC^2-2 code has a more rigorous resonance treatment than does the EPRI-CELL code. Therefore, energy self-shielding factors were used for the ^{238}U resonance capture region and the ^{235}U resonance absorption region. Use of these energy self-sheilding factors effectively replaces the ^{238}U and ^{235}U resonance cross sections generated by EPRI-CELL with those calculated by the MC^2-2 code.

An 11-group cross section set consisting of four fast, three epithermal, and four thermal groups was used for most of the calculations in this study. Some calculations were also performed using the standard five-group structure commonly used at Argonne National Laboratory for MTR plate-type reactor studies. It was found, however, that the five group set did not adequately account for thermal neutron upscattering from excited ZrH energy states in TRIGA fuel. The broad group energy boundaries for both group structures are listed in Table 2.

Different cell models were needed to generate appropriate EPRI-CELL cross sections for the various reactor regions. Once generated, these cross sections sets were combined into one master set and used for multigroup diffusion and transport calculations. Burnup-dependent cross sections were calculated only for isotopes in the fuel pin. Separate unit cell calculations were made for the fuel rod, beryllium reflector, water radial reflector, water axial reflector, internal water-filled flux traps, control rod, and control rod follower.

Most of the results of this study are based on XY multigroup diffusion calculations. Energy-independent axial extrapolation distances derived from flux profiles calculated in an RZ diffusion-theory model were used to account for the axial leakage and power profile. The extrapolation distances used are given in Table 3. Studies have shown that axial buckling values are, to all practical purposes, independent of core temperatures. This is because temperature effects the thermal portion of the neutron spectrum whereas leakage is due mostly to high energy neutrons.

The REBUS-2 fuel cycle analysis code[9] was used to perform burnup calculations. The XY model shown in Fig. 1 was used for the diffusion-theory calculations in REBUS-2. The water thickness outside the beryllium reflector was taken to be 14.68 cm. Except for the outside water pool, each grid position was represented by a uniform 5 × 5 mesh. The use of more mesh intervals was studied briefly. The chief effect was an increase in the eigenvalue by ~0.7% Δk for a doubling of the number of mesh intervals used. The mesh spacing had little effect on calculated flux profiles or control rod worths. Therefore, even though k_{eff} may have been underestimated by up to 1% Δk, the 5 × 5 mesh spacing was used to conserve computer resources. Both non-equilibrium and equilibrium fuel cycle calculations were performed. In the non-equilibrium calculations a core of 40 fresh fuel elements was allowed to burn down with no fuel replacement. In the equilibrium calculations a fixed number of fuel elements were replaced at the end of each cycle and the remaining fuel elements were moved to new locations in the core. After some preliminary studies, a five-path fuel management scheme as given in Table 4, was selected. Cross sections representative of the middle-of-cycle burnup were used in the REBUS-2 calculations. The fuel temperature was assumed to be 800K.

Because of the very strong absorbing quality of the B_4C control rods, the conditions for the valid application of diffusion theory are severely violated, and, therefore, diffusion theory cannot accurately predict control-rod worths. However, approximate control-rod worths can be obtained using diffusion theory with suitable internal boundary conditions calculated from transport theory. The internal group-dependent boundary condition is just the ratio of the neutron current to flux at the surface of the control rod cell. The internal boundary conditions were calcculated for a cell consisting of a control rod surrounded by homogenized fresh fuel using the one-dimensional transport-theory code ONEDANT.[10] To account for flux and scattering anisotropics, the calculations were performed in the P_1S_4 approximation. For the case of a fully-withdrawn rod, the aluminum follower and water were homogenized and normal diffusion theory was used. In order to validate these control-rod-worth calculations, the control rod cell, both with a rod inserted and a rod withdrawn, were calculated using ONEDANT, the VIM Monte Carlo code,[11] and diffusion theory. The results of all three calculations were in excellent agreement.

4. CALCULATIONAL RESULTS

4.1 Fuel Cycle

A plot of k_{eff} vs. integrated reactor power is shown in Fig. 2. The graph shows that once equilibrium concentrations of ^{135}Xe and ^{149}Sm have been reached, k_{eff} increases with burnup until a maximum value is obtained at about 4000 MWd and thereafter decreases with burnup. This behavior results from the fact that the burnable poison, ^{167}Er, burns out faster than ^{235}U. In order to determine the length of such a fuel cycle it is necessary to decide how much excess reactivity is required at the end of cycle. Since the calculations are performed with cross sections representative of hot fuel and with equilibrium xenon and samarium, one needs only that excess reactivity at end of cycle (EOC) sufficient to compensate for the absorption of experiments and to provide for xenon override. In this study it has been assumed that 2% excess is required. Therefore, the non-equilibrium cycle length is calculated to be 8000 MWd (320 full-power days).

The equilibrium fuel cycle is much more economical and results in much smaller reactivity swings and power shifts. For the five-path fuel management scheme described earlier, Fig. 3 shows the end-of-cycle k_{eff} as a function of cycle length. For a fuel temperature of 800K and a 62 day cycle length the beginning-of-cycle (BOC) and EOC eigenvalues were found to be 1.0293 and 1.0194, respectively. For this case, the BOC and EOC ^{235}U and ^{167}Er burnup levels, power generated, and ^{239}Pu generation are tabulated for each fuel element in Tables 5 and 6. For example, the discharged fuel element from the first path generated a power of 0.622 MW, contained 33.3 g ^{239}Pu, and had ^{235}U and ^{167}Er burnup levels of 43.4% and 84.0%, respectively. Of course, if less excess reactivity were to be needed at end of cycle, as, for example, with a small experiment load, a longer cycle length can be obtained. It should be noted that the power sums to ~0.5% less than 25 MW in Tables 5 and 6 because some power is produced by captures in non-fissile regions.

4.2 Neutron Flux Distribution

Thermal ($E_n < 0.625$ eV), epithermal ($0.625 < E_n < 5.53$ keV), and fast (5.53 keV $< E_n < 10.0$ MeV) neutron flux distributions for the beginning of equilibrium cycle (BOC) are plotted in Figs. 4 to 8 for several axial midplane traverses through the core and reflector regions of the MPRR 25 MW LEU TRIGA reactor. Figure 1 shows the location of these traverses which are between columns F and G, at the center of columns H and J, and at the center of row 9. These BOC flux distributions were taken from the two-dimensional XY full-core REBUS calculation corresponding to the 62 day cycle length for a fuel temperature of 800 K with the core operating at 25 MW.

These figures also show EOC/BOC neutron flux ratio distributions. These plots show how the thermal flux in the core regions increases with burnup. The higher average burnup of the core requires that the EOC fluxes be increased relative to the BOC in order to maintain the 25 MW power level.

Maximum and region-averaged thermal fluxes for several irradiation positions are shown in Table 7. Values are given for the BOC and EOC configurations.

Figure 8 shows the flux distribution through row 12 in the pool water region 1.835 cm from the beryllium reflector. Although not modeled in the XY calculations, this is the region where the beam tubes are to be located. Fluxes shown in this figure should be used with caution since they can be expected to be significantly smaller when leakage through the beam tubes is taken into account.

4.3 Safety-Related Parameters

This section presents the results of calculations on safety-related neutronic parameters needed for transient analyses of the 25 MW MPRR LEU TRIGA reactor. These parameters include kinetic parameters (β-effective and the prompt neutron lifetime), prompt negative temperature coefficients, isothermal feedback coefficients and power peaking factors. In most cases calculations were performed for fresh fuel, beginning-of-equilibrium-cycle (BOC) and end-of-equilibrium cycle (EOC) cores for the 62-day cycle-length case.

A.7.1 Kinetic Parameters

The prompt-neutron lifetime (ℓ_p), the neutron generation time (Λ), and the effective delayed-neutron fraction (β_{eff}) were calculated for fresh fuel, BOC, and EOC equilibrium cores using the two-dimensional diffusion theory perturbation capability of the ARC System.[12] Table 8 shows the results of these calculations. For these calculations burnup-dependent atom densities were taken from the REBUS calculation for a cycle length of 62 days. The delayed neutron data, used in the calculation of β_{eff}, were taken from Version V of ENDF/B. Delayed neutron constants for BOC and EOC equilibrium cores are shown in Table 9. All calculations were performed using 11-group cross sections.

4.3.2 The Prompt Negative Temperature Coefficient

One of the characteristics of U-ZrH-Er TRIGA fuel is its large prompt negative temperature coefficent. For small diameter fuel pins, such as those proposed for the MPRR 25 MW TRIGA reactor, the primary contribution to the prompt negative temperature coefficient is a hardening of the thermal neutron spectrum resulting from an increase in the fuel temperature. The binding of the ZrH molecule is described in terms of a harmonic oscillator potential with excited states separated in energy by about 0.14 eV. Thus, the population of excited oscillator states increases with fuel temperature. Thermal neutrons scattered from excited ZrH molecules receive a boost in energy with a subsequent hardening of the neutron spectrum. With this spectral shift toward higher energy, increased absorption in the ~0.5 eV double resonance of ^{167}Er occurs, resulting in a negative reactivity effect. Since the fuel pin is a solid uniform mixture of U-ZrH-Er, the negative reactivity effect as a function of temperature is prompt. This characteristic of TRIGA fuel provides a built-in safety feature in the event of an unplanned power transient.

To evaluate the prompt negative temperature coefficient, 11-group core cross sections were generated at various temperatures using the EPRI-CELL code which was described earlier. Cross sections for H in ZrH were created for temperatures of 296, 500, 800, 1000 and 1200 K using temperature-dependent $S(\alpha,\beta)$ data. Doppler broadening of the ^{238}U resonances, as well as those for the other uranium and plutonium isotopes, was determined by a resonance calculation at each of the above temperatures. However, the EPRI-CELL code does not permit an interpolation on temperature for resonances in the thermal neutron energy range, which is the case for ^{167}Er. Therefore, ^{166}Er and ^{167}Er resonances have been Doppler broadened only at those temperatures for which these cross sections exist in the EPRI-CELL library, namely 293, 564, 886, 1100, and 1200 K. Thus, a mismatch exists between the temperatures for which the erbium resonances have been Doppler broadened and the temperatures at which the H (in ZrH), U and Pu cross sections apply. This mismatch is summarized below.

Temperature (K) for H in ZrH and for Doppler-Broadened U and Pu Resonances	Temperature (K) for Doppler-Broadened Er Resonances
296	293
500	564
800	886
1000	1100
1200	1200

Except for Zr, all other core materials were assumed to remain at room temperature.

The core-isothermal prompt negative temperature coefficients were calculated for fresh fuel atom densities and cross sections and for REBUS atom densities corresponding to the BOC and EOC configurations for the 62-day cycle-length case. For these calculations it was assumed that the changes in core temperature are independent of position. The effect of this approximation on the value of the temperature coefficient is thought to be small, but has not been investigated.

Diffusion theory calculations of k_{eff} at each ZrH temperature were made using the XY model of the 25 MW MPRR TRIGA Reactor (Fig. 1) and the appropriate 11-group temperature-dependent cross sections. It was assumed that all control rods are fully withdrawn, experiment regions are water-filled, the fuel pin composition is at the specified temperature, and all other materials are at room temperature. It was also assumed that the axial bucklings are independent of temperature.

The calculated values of k_{eff} were fitted by the least squares process to a 3rd degree polynomial in temperature and the prompt negative temperature coefficient (α_p) was evaluated as the derivative of the polynomial. The prompt negative temperature coefficient decreases as a function of burnup because of the depletion of ^{167}Er in the fuel.

4.3.3 Equilibrium ^{135}Xe and ^{149}Sm Worths

The reactivity worths of equilibrium concentrations of ^{135}Xe and ^{149}Sm were evaluated for the BOC configuration using REBUS-calculated atom densities for the case of a 62 day cycle length at a fuel temperature of 800K. Table 10 gives the results.

4.3.4 Isothermal Reactivity Feedback Coefficients

Isothermal feedback coefficients were evaluated for the combined effects of temperature and density changes in the water moderator. These reactivity changes are the results of two physical effects:

1. The hardening of the thermal neutron spectrum resulting from an increase in the water temperature.

2. The increase in neutron leakage resulting from a reduction in the density of the water as it heats (or boils).

Using 11-group cross sections generated for various water temperatures in the core, XY diffusion calculations were performed with fresh fuel atom densities to evaluate the feedback coefficients. Table 11 shows the feedback coefficients for the combined effects of temperature and water density changes. In this table, $\delta\rho = (k_2 - k_1)/k_1k_2$ is the change in reactivity related to changes in core water temperature and density. The temperature and density of the reflector and flux trap water were not allowed to vary. RZ calculations were performed at each water density to determine the axial extrapolation distances needed for the XY calculations.

4.3.5 Power Peaking Factors

Radial, axial, and local power peaking factors have been calculated for the MPRR LEU TRIGA for the beginning-of-cycle (BOC) and end-of-cycle (EOC) equilibrium core. The radial peaking factor, F_r, is the ratio of the power density at the hot spot on the axial midplane to the average midplane power density, as calculated in XY diffusion theory problems. The axial peaking factor, F_a, is just the peak-to-average value of the chopped cosine axial shape. The local peaking factor, F_ℓ, is the radial peak-to-average power density in the local fuel element. Finally, the total peaking factor is the product of these three components.

Peaking factors were evaluated for BOC and EOC equilibrium cores. The hot spot is in fuel element FE9G (see Fig. 1) adjacent to the water-filled irradiation hole ES9H. Power peaking factors are given in Table 12. These are over-pessimistic values since in actual practice the irradiation positions would be filled with aluminum or beryllium blocks containing small holes to accomodate samples so as to minimize power peaking effects. Figure 11 shows how the power density varies in the X and Y directions across fuel element FE9G. The Y-traverse is 0.734 cm from the core-water interface. Note the very large power peak in fuel next to the water-filled irradiation hole.

4.4 Control Rod Worths

The results of the control rod worth calculations are summarized in Table 13. In the BOC configuration, rod C9F is the most reactive; when it is stuck out, the worth of the remaining five rods is 6.47% $\delta\rho$. In the beginning-of-cycle condition the five inserted rods should be able to shut down the reactor with all experiments removed, with all xenon decayed, and with the fuel cold. For the 62-day cycle-length case, the BOC excess reactivity is 2.85% $\delta\rho$ with an 800 K fuel temperature (Section 4.1), the xenon worth is 2.50% $\delta\rho$ (table 10), and the increase in reactivity upon cooling of the fuel meat to room temperature is 1.92% $\delta\rho$ (Fig. 9), giving a maximum excess reactivity of 7.27% $\delta\rho$. Therefore, if the control rod worth calculations are correct, there is not an adequate shutdown margin when one rod is stuck out of the core. Also, the fresh core has an inadequate shutdown margin with one rod stuck. In relation to the accuracy of the control rod worth calculations it must be emphasized that no comparisons with measured data have been made for control rod worths in LEU TRIGA cores. However, the same methods for individual borated stainless steel rods in the LEU core of the Ford Nuclear Reactor at The University of Michigan yielded worths within 0.2% $\delta\rho$ of the measured values.[17]

Higher-worth control rods of a different design could be considered. For example, higher worth rods would result if the borated stainless steel poison material were in the shape of a square annulus about 7 cm on a side and 1 cm thick with a water hole at the center. The water hole serves to thermalize and trap fast neutrons which penetrate the borated stainless steel annulus. Relative to the cylindical rod, the square shape of the borated stainless steel absorber provides a greater surface area and this too tends to increase the value of the rod worth. However, no calculations were made for the worth of control rods of this design.

5. CONCLUSIONS

In all aspects except for the shutdown margin, the 25-MW LEU TRIGA Multipurpose Research Reactor performs very well. The high uranium density of the U-ZrH-Er fuel with its burnable poison makes possible a long equilibrium cycle length with a relatively small reactivity swing. Therefore, control rod movement is minimized during the cycle, leading to a stable flux. The lack of adequate shutdown margin can probably be remedied by the use of a higher-worth design of the control rods.

References

1. The 25-MW TRIGA Multipurpose Research Reactor for the Bandung Research Center, Bandung, Indonesia, General Atomic Company.

2. Guidebook on "Research Reactor Core Conversion from the Use of Highly Enriched Uranium to the Use of Low Enriched Uranium Fuels," International Atomic Energy Agency Report IAEA-TECDOC-233, (August 1980).

3. B. A. Zolotar, et al., "EPRI-CELL Code Description, "Advanced Recycle Methodology Program System Documentation, Part II, Chapter 5, Electric Power Research Institute (September 1977).

4. G. D. Joanou and J. S. Dudek, "GAM-I: A Consistent P_1 Multigroup Code for the Calculation of Fast Neutron Spectra and Multigroup Constants," General Atomic Company Report GA-1850 (June 1961).

5. H. C. Honeck, "THERMOS, A Thermalization Transport Theory Code for Reactor Lattice Calculations," Brookhaven National Laboratory Report BNL-5826 (September 1961).

6. H. Henryson III, B. J. Toppel, and C. G. Stenberg, "MC^2-2: A Code to Calculate Fast Neutron Spectra and Multigroup Cross Sections," Argonne National Laboratory Report ANL-8144 (June 1976).

7. N. M. Greene, et al., "AMPX: A Modular Code System for Generating Coupled Multigroup Neutron and Gamma Libraries from ENDF/B," Oak Ridge National Laboratory Technical Memorandum ORNL-TM-3706 (November 1974).

8. R. E. MacFarlane, et al., "The NJOY Nuclear Data Processing System: User's Manual," Los Alamos Scientific Laboratory Report LA-7584-M (December 1978).

9. R. B. Hosteny, "The ARC System Fuel Cycle Analysis Capability, REBUS-2," Argonne National Laboratory Report ANL-7721 (1978).

10. R. D. O'Dell, F. W. Brinkley and D. R. Marr, "Users' Manual for ONEDANT: A Code Package for One-Dimensional Diffusion-Accelerated, Neutral-Particle Transport," Los Alamos Scientific Laboratory, October 1980.

11. R. E. Prael and L. J. Milton, "A User's Manual for the Monte Carlo Code VIM," Argonne National Laboratory Technical Memorandum FRAM-TM-84 (February 1976).

12. T. A. Daly, C. G. Stenberg, D. E. Neal, D. A. Schoengold, and G. K. Leaf, "The ARC System Two-Dimensional Adjunct Calculations," Argonne National Laboratory Report ANL-7722 (October 1972).

13. M. M. Bretscher and J. L. Snelgrove, "Comparison of Calculated with Measured Quantities for the LEU-Fueled Ford Nuclear Reactor," International Meeting on Research and Test Reactor Core Conversions from HEU to LEU Fuels, Argonne, Illinois, November 8-10, 1982 (to be published).

Table 1. Data For The 36-Rod TRIGA Fuel Cluster

Parameter	Design Value
Fuel Diameter (unclad)	0.853 cm (0.336 in.)
Rod Diameter (with clad)	0.914 cm (0.360 in.)
Rod-Rod Clearance	0.203 cm (0.080 in.)
Rod-shroud Clearance	0.203 cm (0.080 in.)
Shroud Side Dimension	7.214 cm (2.840 in.)
Lattice Pitch	7.341 cm (2.890 in.)
Fuel Length	55.88 cm (22.0 in.)
Fuel Composition:	$U\text{-}Er\text{-}ZrH_{1.6}$
Uranium Content	45 wt%
Er Content	1.5 wt%
^{235}U Enrichment	19.9 atom %
Hydrogen-to-Zironium Ratio	1.6
Fuel Pin Loading:	
Uranium	119.12 g
^{235}U	23.71 g
Erbium (natural)	4.0 g
^{167}Er	0.91 g
Fuel Cluster (36 Rods) Loading:	
Uranium	4.29 kg
U-235	0.853 kg
Erbium (natural)	0.143 kg
^{167}Er	32.8 g

Table 2. Group Structure for 5- and 11-Broad-Group Cross Section Sets

Group Number	Upper Energy of Group (eV) (5-Group Set)	Upper Energy of Group (eV) (11-Group Set)
1	1.0000E+7	1.0000E+7
2	8.2085E+5	8.2085E+5
3	5.5309E+3	6.3928E+5
4	1.8550	9.1188E+3
5	6.2493E-1	5.5308E+3
6		1.8550
7		1.1664
8		6.2493E-1
9		4.1704E-1
10		1.4573E-1
11		5.6925E-2

Table 3. Extrapolation Distances and Corresponding Bucklings

Quantity	Reactor Region					
	Core	Outer Flux Trap	Inner Flux Trap	Control Rod Follower	Beryllium Reflector	Pool Water
5 Group Structure:						
δ_z, cm	5.560	5.504	5.511	6.524	6.089	5.895
B_z^2, cm^{-2}	2.1986E-3	2.2060E-3	2.2051E-3	2.0773E-3	2.1308E-3	2.1553E-3
11 Group Structure:						
δ_z, cm	5.550	5.471	5.476	6.714	6.162	5.955
B_z^2, cm^{-2}	2.1999E-3	2.2103E-3	2.2097E-3	2.0546E-3	2.1217E-3	2.1477E-3

Table 4. Fuel Element Positions Arranged in the Order of Increasing Burnup for the Five Path Fuel Management Scheme*

Path:	I	II	III	IV	V
Burnup Stage					
1	FE10E	FE10F	FE10G	FE9E	FE8C
2	FE7C	FE9D	FE8I	FE6C	FE4H
3	FE6J	FE5J	FE7J	FE5D	FE8J
4	FE5C	FE8E	FE3H	FE7D	FE3G
5	FE6I	FE3F	FE4I	FE5H	FE10H
6	FE9G	FE3E	FE9I	FE8F	FE7E
7	FE8H	FE8G	FE4D	FE7H	FE6H
8	FE6E	FE5G	FE4I	FE5E	FE5F

*The five columns give the fuel shuffling sequence from top to bottom.

Table 5. BOC Fuel Element ^{235}U Mass, ^{167}Er Mass, Burnup and Power for the MPRR 25MW LEU TRIGA Reactor

Case: Fuel Temp = 800K, Cycle Length = 62 days days, k_{eff}(EOC) = 1.019

Fuel Management Path	Stage	Region	^{235}U Mass g	^{167}Er Mass g	^{235}U Burnup %	^{167}Er Burnup %	Power MW	^{238}U Mass g	^{239}Pu Mass g
I	1	FE10E	849	32.7	0.0	0.0	0.572	3438	0.0
"	2	FE7C	801	26.9	5.6	17.8	0.624	3431	6.8
"	3	FE6J	753	21.3	11.3	34.9	0.639	3421	13.9
"	4	FE5C	705	16.8	16.9	48.7	0.580	3411	19.8
"	5	FE6I	663	13.7	21.9	58.1	0.637	3403	23.3
"	6	FE9G	617	10.7	27.3	67.4	0.665	3393	27.6
"	7	FE8H	569	8.3	33.0	74.6	0.659	3382	30.3
"	8	FE6E	523	6.5	38.4	80.1	0.622	3372	32.2
II	1	FE10F	849	32.7	0.0	0.0	0.573	3438	0.0
"	2	FE9D	801	26.4	5.6	19.2	0.640	3430	7.7
"	3	FE5J	751	21.2	11.5	35.4	0.641	3421	13.9
"	4	FE8E	703	16.9	17.1	48.5	0.622	3412	19.2
"	5	FE3F	656	13.1	22.6	59.9	0.565	3401	24.4
"	6	FE3E	616	10.6	27.4	67.7	0.610	3392	27.8
"	7	FE8G	572	8.6	32.6	73.8	0.652	3384	29.5
"	8	FE5G	526	6.7	38.0	79.4	0.622	3374	31.4
III	1	FE10G	849	32.7	0.0	0.0	0.573	3438	0.0
"	2	FE8I	801	26.4	5.6	19.2	0.623	3430	7.7
"	3	FE7J	754	20.9	11.2	36.1	0.644	3420	14.6
"	4	FE3H	706	16.5	16.8	49.6	0.590	3410	20.3
"	5	FE4I	663	13.5	21.9	58.9	0.625	3402	23.8
"	6	FE9I	618	10.8	27.2	67.0	0.672	3394	26.8
"	7	FE4D	570	8.6	32.9	73.6	0.612	3385	28.5
"	8	FE4F	527	7.0	37.9	78.5	0.611	3377	30.0
IV	1	FE9E	849	32.7	0.0	0.0	0.598	3438	0.0
"	2	FE6C	800	26.0	5.8	20.5	0.625	3429	8.3
"	3	FE5D	752	20.7	11.4	36.7	0.585	3419	14.9
"	4	FE7D	707	16.5	16.6	49.5	0.634	3410	20.3
"	5	FE5H	660	12.9	22.2	60.6	0.616	3400	25.3
"	6	FE8F	616	10.1	27.4	69.0	0.673	3390	29.0
"	7	FE7H	568	7.9	33.1	75.8	0.666	3376	31.3
"	8	FE5E	522	6.2	38.5	80.9	0.608	3370	32.8
V	1	FE8C	849	32.7	0.0	0.0	0.637	3438	0.0
"	2	FE4H	797	26.2	6.1	20.0	0.603	3429	7.8
"	3	FE8J	751	20.8	11.5	36.3	0.624	3420	14.6
"	4	FE3G	704	16.8	17.0	48.5	0.590	3412	19.3
"	5	FE10H	661	13.5	22.1	58.8	0.629	3402	23.7
"	6	FE7E	614	10.8	27.6	66.9	0.665	3394	26.4
"	7	FE6H	567	8.4	33.2	74.2	0.652	3384	29.3
"	8	FE5F	521	6.7	38.6	79.6	0.607	3374	31.3
Total:			27379	678.8	19.3	48.1	24.886	136247	773.7

Table 6. EOC Fuel Element ^{235}U Mass, ^{167}Er Mass, Burnup and Power for the MPRR 25MW LEU TRIGA Reactor

Case: Fuel Temp = 800K, Cycle Length = 62 days days, k_{eff}(EOC) = 1.019

Fuel Management Path	Stage	Region	235U Mass g	167Er Mass g	235U Burnup %	167Er Burnup %	Power MW	238U Mass g	239Pu Mass g
I	1	FE10E	801	26.9	5.6	17.9	0.573	3430	6.8
"	2	FE7C	753	21.3	11.3	34.9	0.625	3421	13.9
"	3	FE6J	705	16.8	16.9	48.7	0.639	3411	19.8
"	4	FE5C	663	13.7	21.9	58.1	0.580	3403	23.3
"	5	FE6I	617	10.7	27.3	67.4	0.636	3393	27.6
"	6	FE9G	569	8.3	33.0	74.6	0.665	3382	30.3
"	7	FE8H	523	6.5	38.4	80.1	0.659	3372	32.2
"	8	FE6E	480	5.2	43.4	84.0	0.622	3362	33.3
II	1	FE10F	801	26.4	5.6	19.2	0.575	3430	7.7
"	2	FE9D	751	21.2	11.5	35.4	0.641	34321	13.9
"	3	FE5J	703	16.9	17.1	48.5	0.640	3412	19.2
"	4	FE8E	656	13.1	22.6	59.9	0.623	3401	24.4
"	5	FE3F	616	10.6	27.4	67.7	0.565	3392	27.7
"	6	FE3E	572	8.6	32.6	73.8	0.610	3384	29.5
"	7	FE8G	526	6.7	38.0	79.4	0.653	3374	31.4
"	8	FE5G	484	5.4	43.0	83.5	0.622	3364	32.6
III	1	FE10G	801	26.4	5.6	19.2	0.574	3430	7.7
"	2	FE8I	754	20.9	11.3	36.1	0.623	3420	14.6
"	3	FE7J	706	16.5	16.9	49.6	0.643	3410	20.3
"	4	FE3H	663	13.5	21.9	58.9	0.590	3402	23.8
"	5	FE4I	618	10.8	27.3	67.0	0.625	3394	26.8
"	6	FE9I	570	8.6	33.0	73.6	0.672	3385	28.5
"	7	FE4D	527	7.0	37.9	78.5	0.611	3377	29.6
"	8	FE4F	485	5.6	42.9	82.8	0.610	3367	31.4
IV	1	FE9E	780	26.0	5.8	20.5	0.599	3429	8.3
"	2	FE6C	752	20.7	11.4	36.7	0.625	3419	14.9
"	3	FE5D	708	16.5	16.6	49.5	0.585	3410	20.3
"	4	FE7D	660	12.9	22.2	60.6	0.634	3400	25.3
"	5	FE5H	616	10.1	27.4	69.0	0.615	3390	29.0
"	6	FE8F	568	7.9	33.1	75.8	0.674	3380	31.3
"	7	FE7H	522	6.2	38.5	80.9	0.665	3370	32.8
"	8	FE5E	481	5.0	43.4	84.6	0.607	3360	33.9
V	1	FE8C	797	26.2	6.1	20.0	0.638	3429	7.8
"	2	FE4H	751	20.8	11.5	36.3	0.603	3420	14.6
"	3	FE8J	704	16.8	17.0	48.5	0.624	3412	19.3
"	4	FE3G	661	13.5	22.1	58.8	0.589	3402	23.7
"	5	FE10H	614	10.8	27.6	66.9	0.630	3394	26.4
"	6	FE7E	567	8.4	33.2	74.2	0.665	3384	29.3
"	7	FE6H	521	6.7	38.6	79.6	0.652	3374	31.3
"	8	FE5F	480	5.4	43.4	83.6	0.606	3364	32.5
Total:			25545	541.8	24.7	58.6	24.876	135873	937.4

Table 7. Thermal Neutron Fluxes (E_n < 0.625 eV) in the Axial Midplane for the 25 MW LEU TRIGA Reactor

		BOC, $\times 10^{14}/cm^2$-sec		EOC, $\times 10^{14}/cm^2$-sec	
Region	Comp.	Max.	Ave.	Max.	Ave.
E67FG	H_2O	4.49	2.62	4.50	2.64
ES9H	H_2O	3.79	2.18	3.77	2.17
RFL11F	Be	1.28	0.80	1.23	0.77
RFL2F	Be	1.22	0.79	1.27	0.83

Table 8. MPRR 25 MW LEU TRIGA Reactor Kinetic Parameters

Quantity	Fresh Fuel K = 1.086366	BOC	EOC
Fuel Temperature, °K	296	800	800
Neutron Generation Time, μs	28.62	31.23	32.15
Prompt Neutron Lifetime, μs	31.09	32.11	32.74
Effective Delayed Neutron Fraction	0.00733	0.00696	0.00687

Table 9. Delayed Neutron Parameters for the MPRR 25 MW LEU TRIGA Reactor

	Beginning-of-Equilibrium Cycle		End-of-Equilibrium Cycle	
Group, i	λ_i, s^{-1}	β_i	λ_i, s^{-1}	β_i
1	1.2730-02	2.5971-04	1.2732-02	2.5562-04
2	3.1716-02	1.4774-03	3.1705-02	1.4606-03
3	1.1703-01	1.3060-03	1.1718-01	1.2893-03
4	3.1284-01	2.8139-03	3.1306-01	2.7719-03
5	1.3984	9.0938-04	1.3982	8.9728-04
6	3.8558	1.9309-04	3.8427	1.9098-04
Total:		6.9595-03		6.8657-03

Table 10. ^{135}Xe and ^{149}Sm Reactivity Worths Beginning-of-Equilibrium Cycle MPRR 25 MW LEU TRIGA Reactor

Condition	k_{eff}
BOC with ^{135}Xe and ^{149}Sm	1.02953
BOC without ^{135}Xe	1.05671
BOC Without ^{149}Sm	1.03605

	^{135}Xe	^{149}Sm
Reactivity Worth, δk-%	2.72	0.65
δρ-%	2.50	0.61

Note: $\delta\rho \equiv \frac{k_1 - k_2}{k_1 k_2}$

Table 11. MPRR LEU TRIGA Isothermal Feedback Coefficients for the Combined Effect of Water Temperature and Density Changes

T_{H_2O}, °C	ρ_{H_2O} g/cm^3	k_{eff}	$-\delta\rho \times 1000$
23	0.998	1.08509	-
60	0.983	1.08061	3.82
77	0.974	1.08021	4.16
127	0.900	1.06617	16.35

Table 12. Radial, Axial, and Local Power Peaking Factors for the MPRR 25 MW LEU TRIGA Reactor Equilibrium Core

Peaking Factor	BOC	EOC
Radial, F_r	1.692	1.629
Axial, F_a	1.355	1.355
Local, F_ℓ	1.532	1.528
Total:	3.512	3.373

Table 13. Control Rod Worths for the MPR 25 MW LEU TRIGA Reactor

	Fresh Fuel Fuel Temp. = 296 K Mod. Temp. = 298 K			BOC Fuel Temp. = 800 K Mod. Temp. = 298 K			EOC Fuel Temp. = 800 K Mod. Temp. = 298 K		
Position of Rods	k_{eff}	δk-%	δρ-%	k_{eff}	δk-%	δρ-%	k_{eff}	δk-%	δρ-%
All B_4C Rods Out	1.08775			1.02953			1.01963		
All B_4C Rods In	0.99373	9.40	8.70	0.93469	9.48	9.86	0.92381	9.58	10.17
C4G Out, Others In	1.02325	6.45	5.79	0.96029	6.92	7.00	0.95050	6.92	7.14
C9F Out, Others In	1.01834	6.94	6.27	0.96520	6.43	6.47	0.95199	6.76	6.97
C6D Out, Others In	1.02021	6.75	6.09	0.95922	7.03	7.12	0.94984	6.98	7.20
C7I Out, Others In	1.01969	6.81	6.14	0.96256	6.70	6.76	0.95322	6.64	6.83
C8D Out, Others In	1.00697	8.08	7.37	0.95130	7.82	7.99	0.94058	7.90	8.24
C5I Out, Others In	1.00812	7.96	7.26	0.95002	7.95	8.13	0.94073	7.89	8.23

Note: $\delta\rho \equiv \frac{k_1 - k_2}{k_1 k_2}$

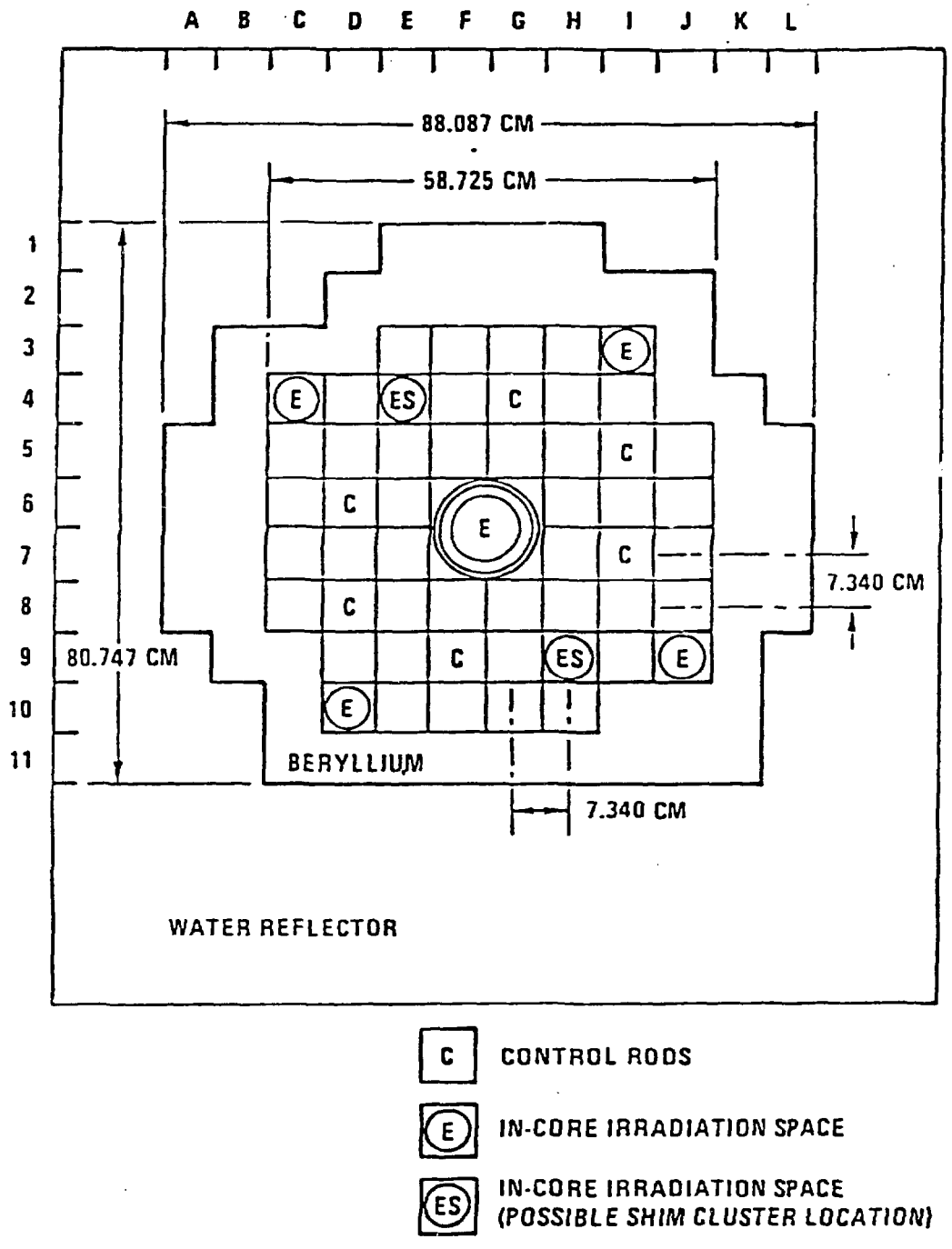

Fig. 1. XY Model of the 25-MW TRIGA Multipurpose Research Reactor (Figure taken from Ref. 1)

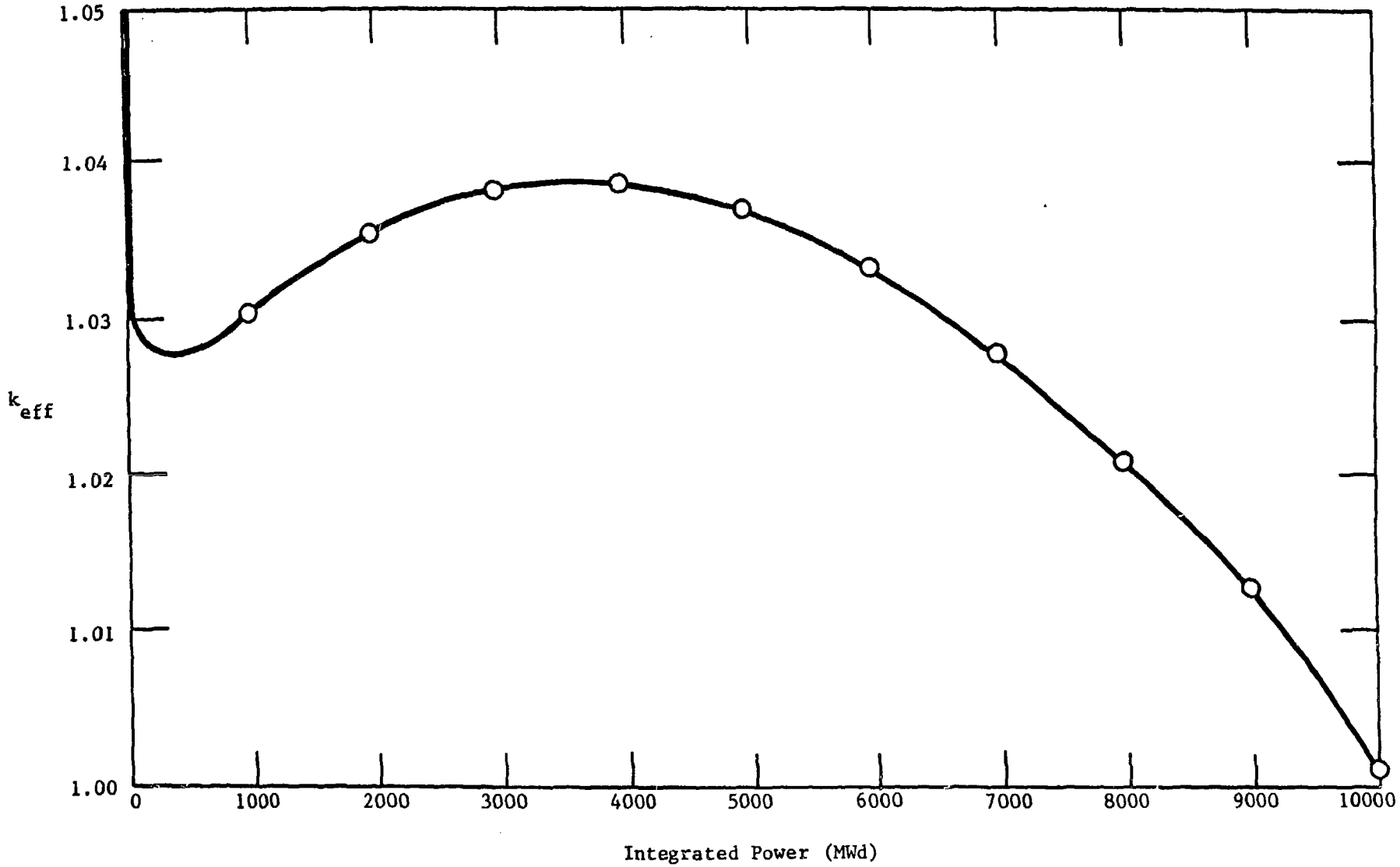

Fig. 2 k_{eff} as a function of reactor integrated power for the non-equilibrium fuel cycle.

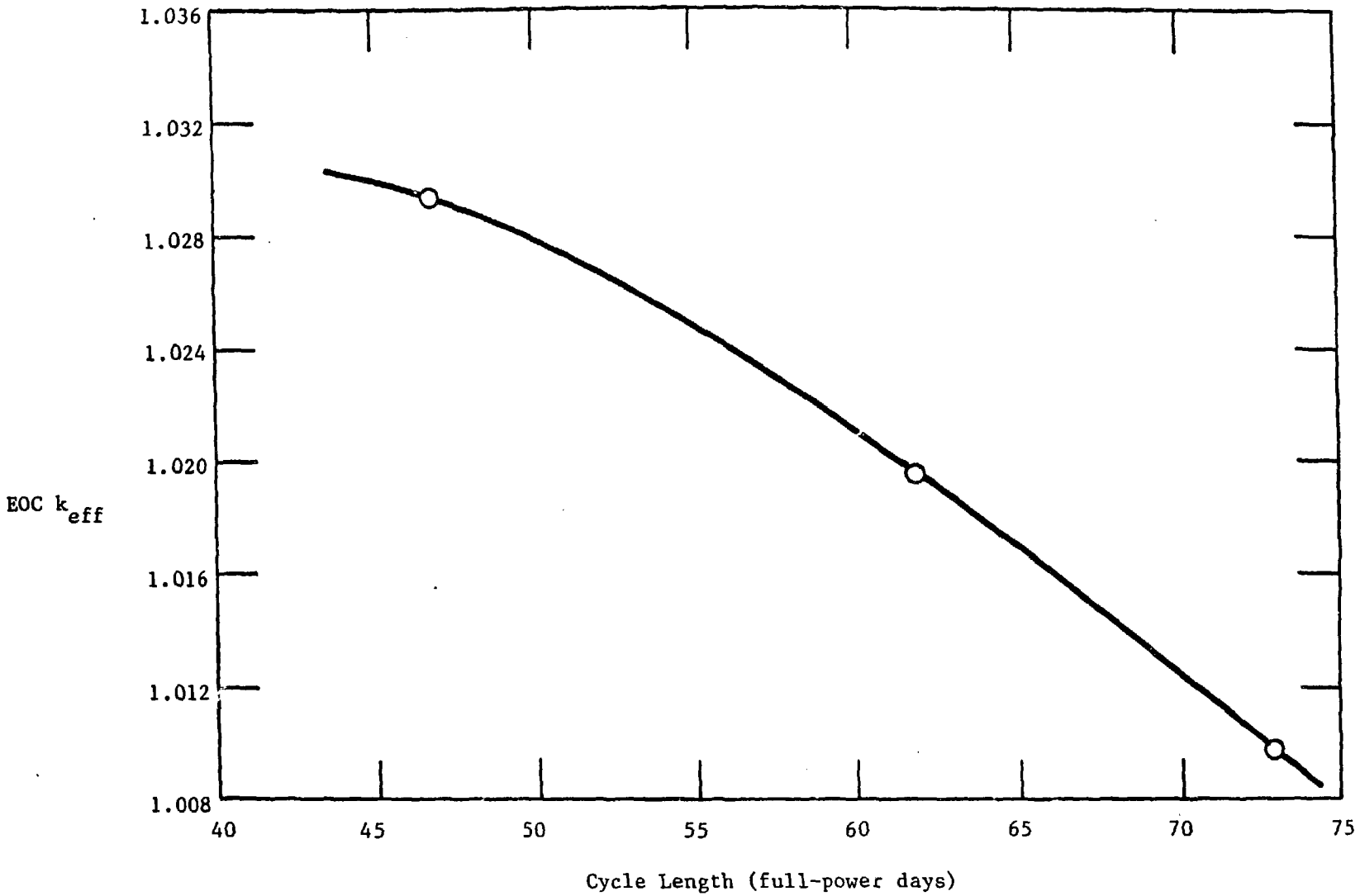

Fig. 3 EOC k_{eff} as a function of fuel cycle length for the five-path fuel management scheme.

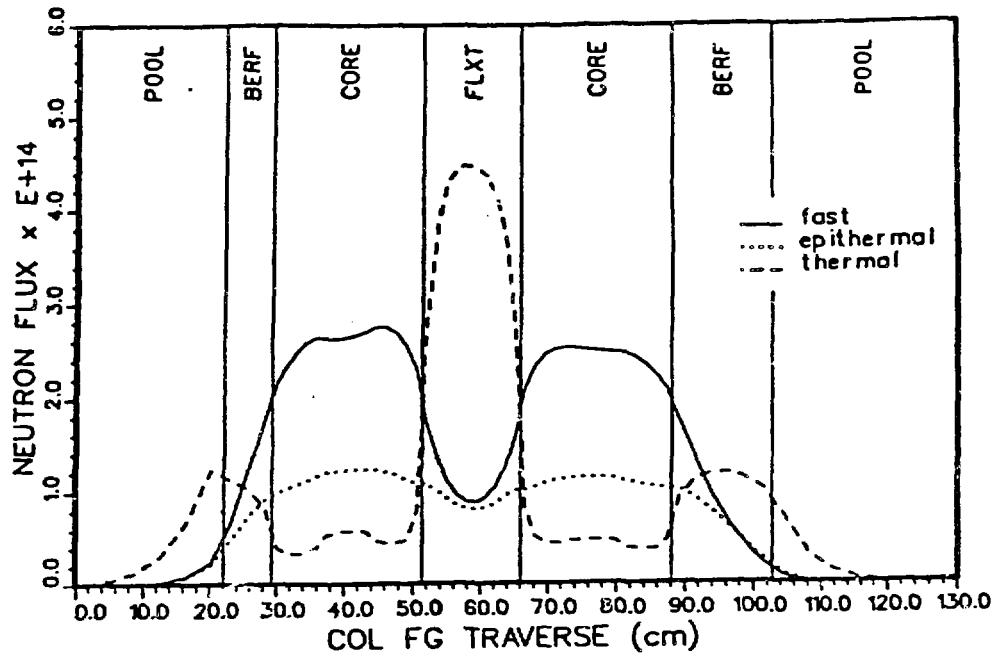

Fig. 4a. MPRR 25 MW LEU TRIGA Core with Water Filled Central Flux Trap. Beginning of Equilibrium Cycle (BOC) Midplane Flux Traverses are Between Columns F and G.

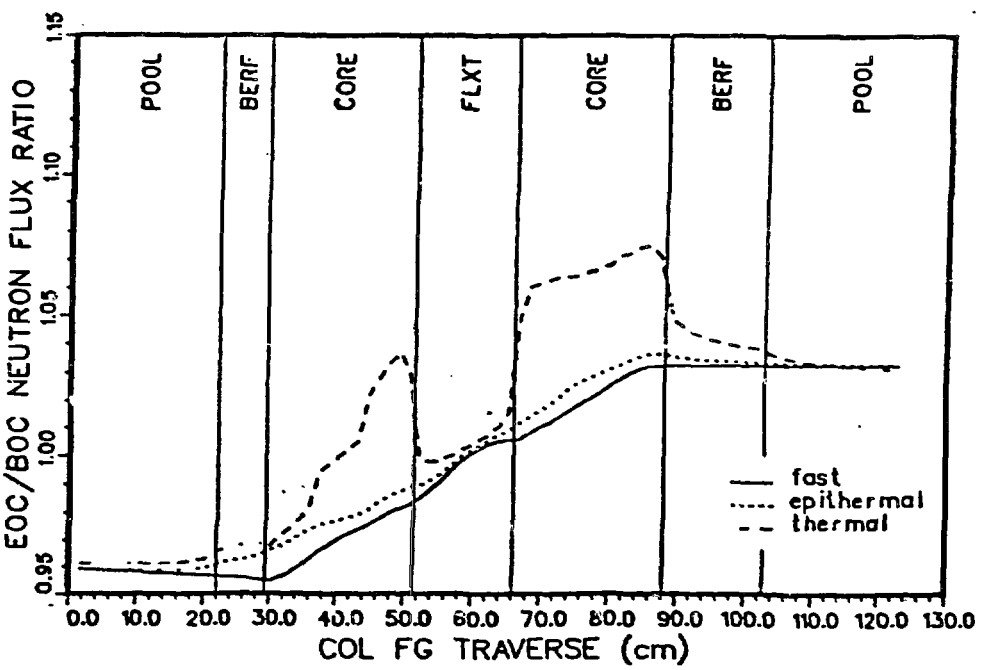

Fig. 4b. End of Cycle to Beginning of Cycle (EOC/BOC) Flux Ratio Distributions in Midplane Between Columns F and G.

Fast Flux: $5.53\ \text{keV} \leq E_n \leq 10.0\ \text{MeV}$

Epithermal Flux: $0.625\ \text{eV} \leq E_n \leq 5.53\ \text{KeV}$

Thermal Flux: $0.0\ \text{eV} \leq E_n \leq 0.625\ \text{eV}$

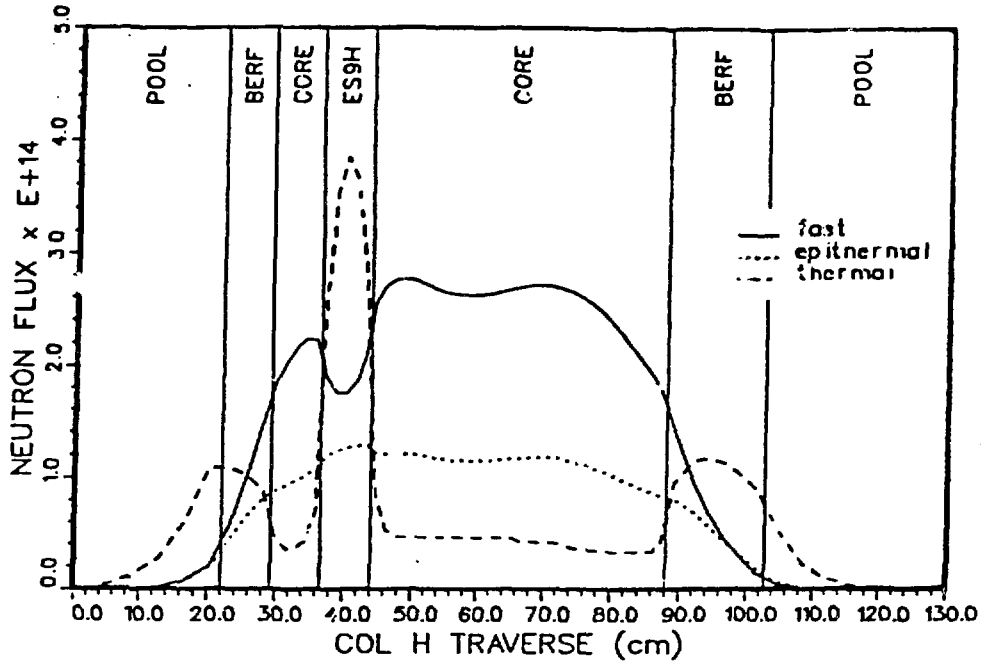

Fig. 5a. MPRR 25 MW LEU TRIGA Core with Water-Filled Experiment Regions. BOC Midplane Flux Distribution is at the Center of Column H.

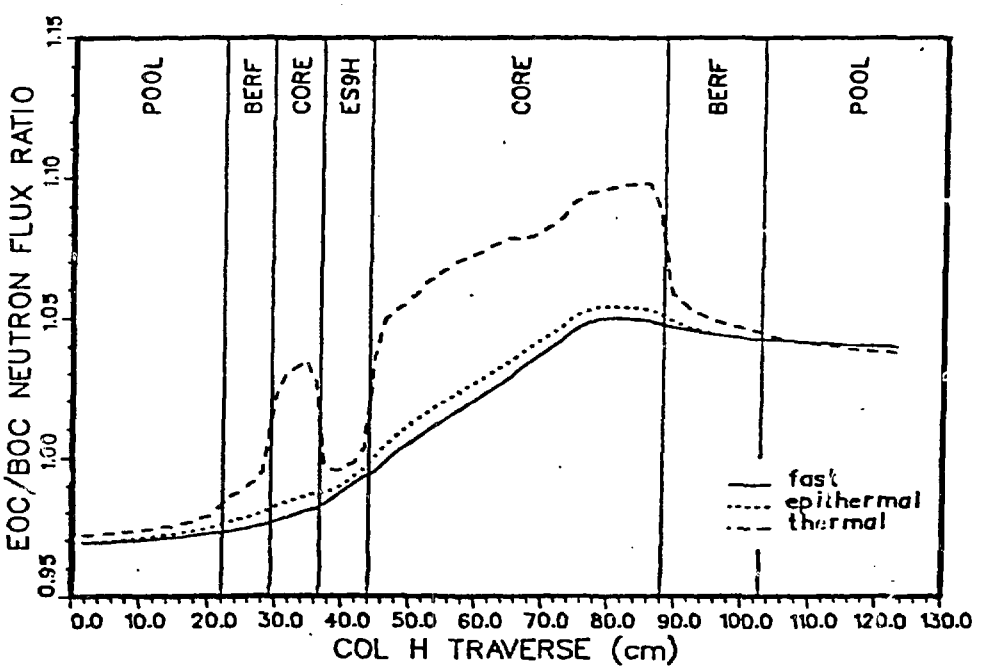

Fig. 5b. EOC/BOC Midplane Flux Ratio Distribution at the Center of Column H.

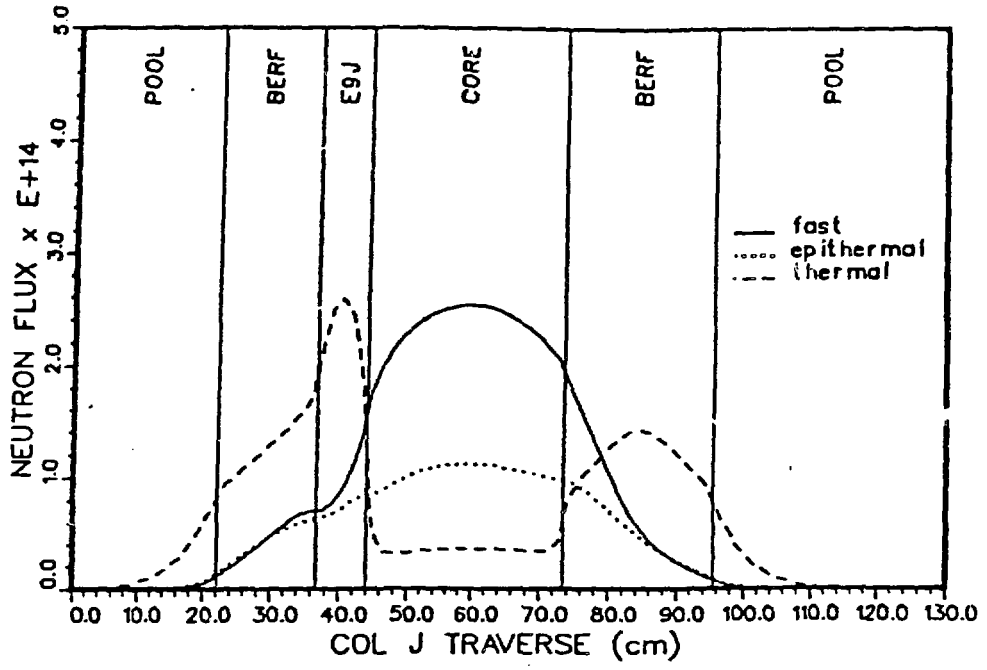

Fig. 6a. MPRR 25 MW LEU TRIGA Core with Water-Filled Experiment Regions. BOC Midplane Flux Distribution is at the Center of Column J.

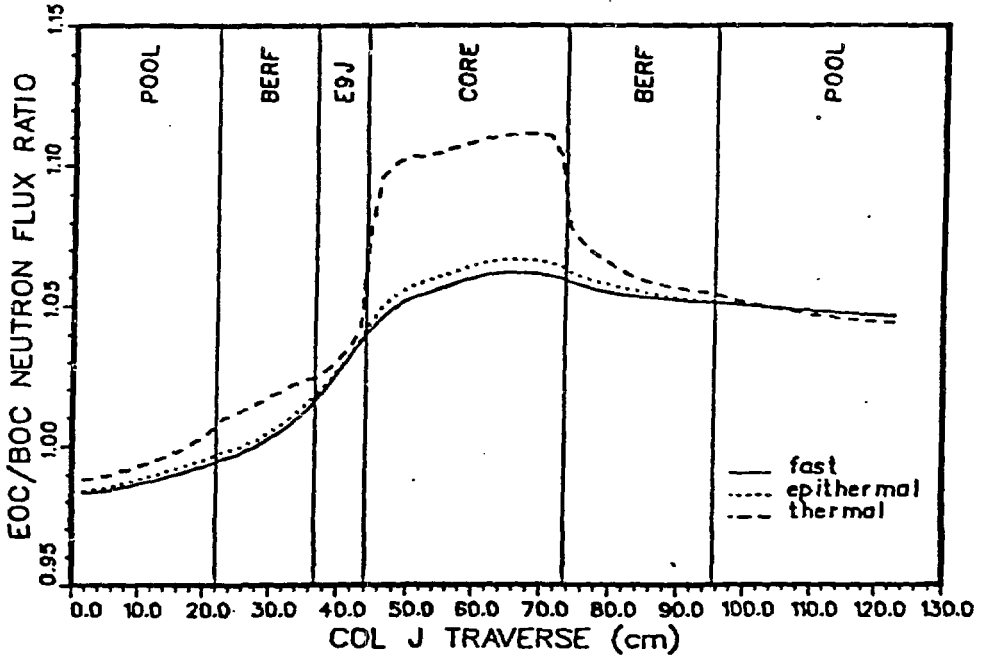

Fig. 6b. EOC/BOC Midplane Flux Ratio Distribution at the Center of Column J.

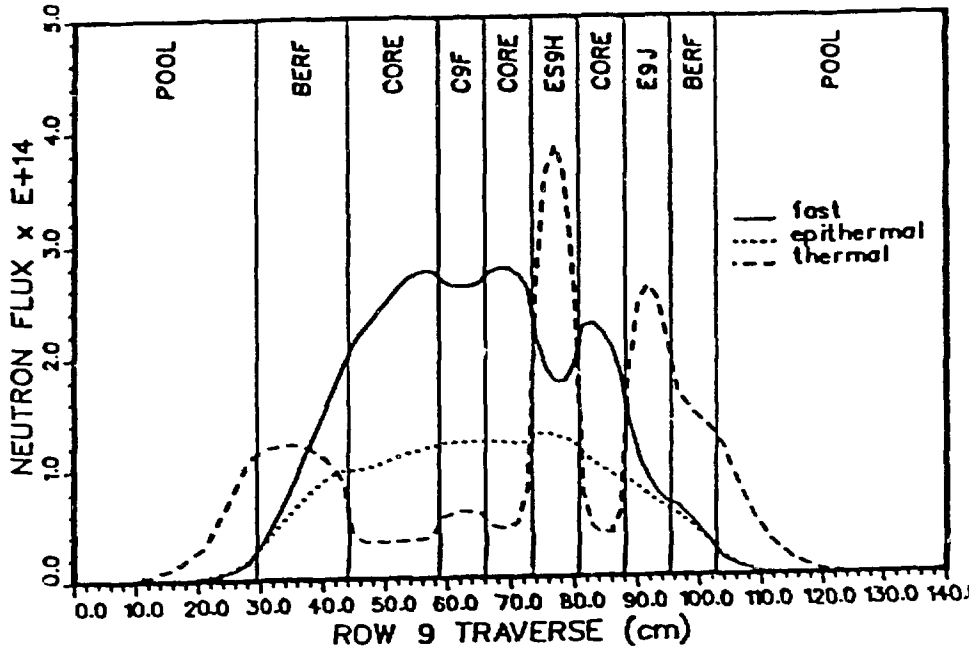

Fig. 7a. MPRR 25 MW LEU TRIGA Core with Water-Filled Experiment Regions. BOC Midplane Flux Distribution is at the Center of Row 9.

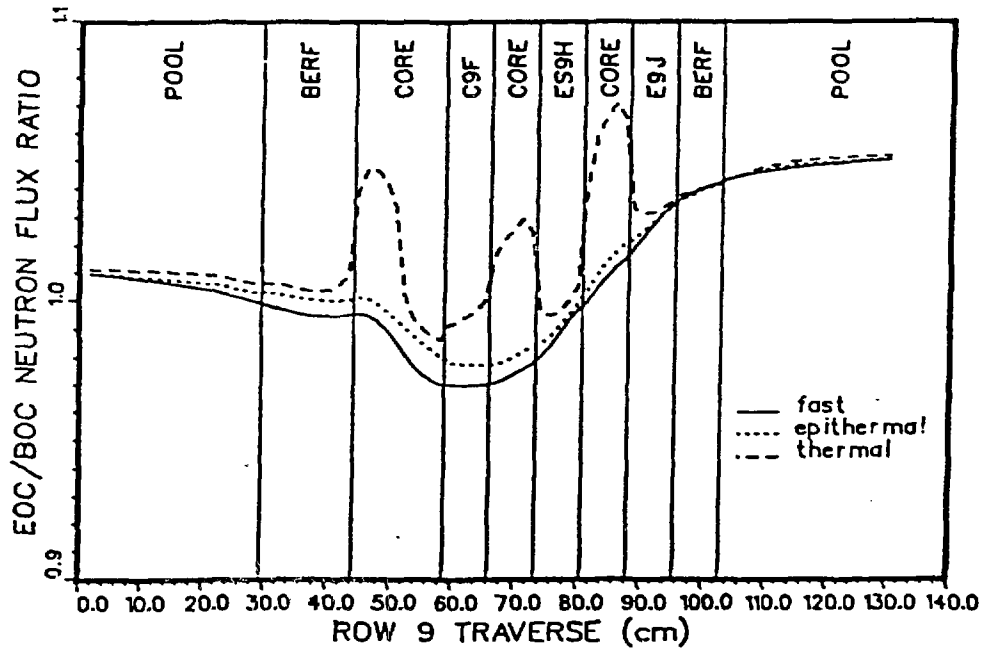

Fig. 7b. EOC/BOC Midplane Flux Ratio Distribution at the Center of Row 9.

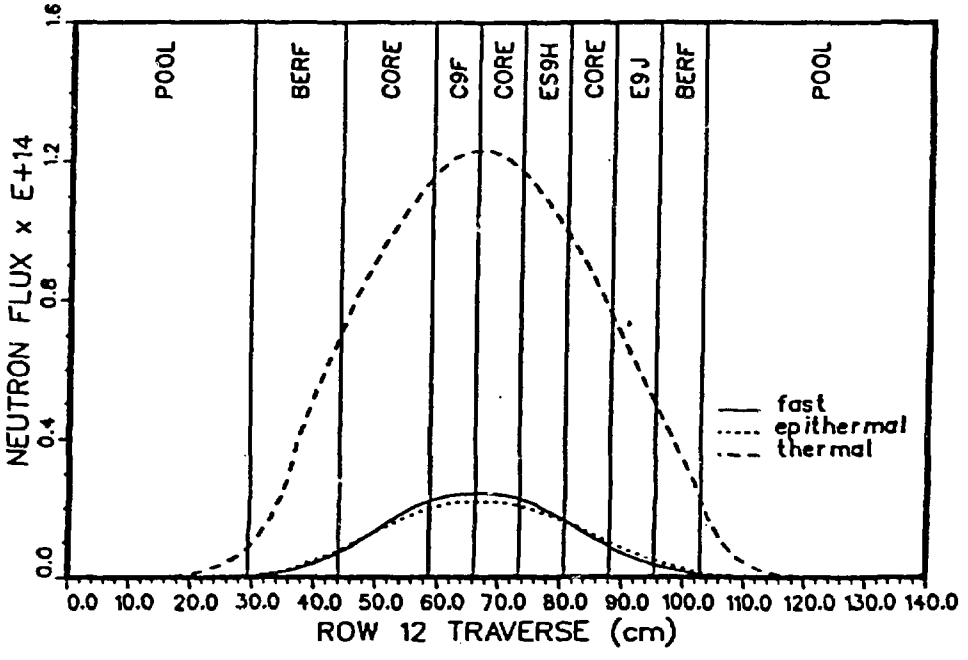

Fig. 8. BOC Midplane Flux Distributions Through Row 12 in the Water Reflector Region Adjacent to the Beryllium Reflector for the MPRR LEU TRIGA Reactor. This is the Region Where Beam Tubes Would be Located.

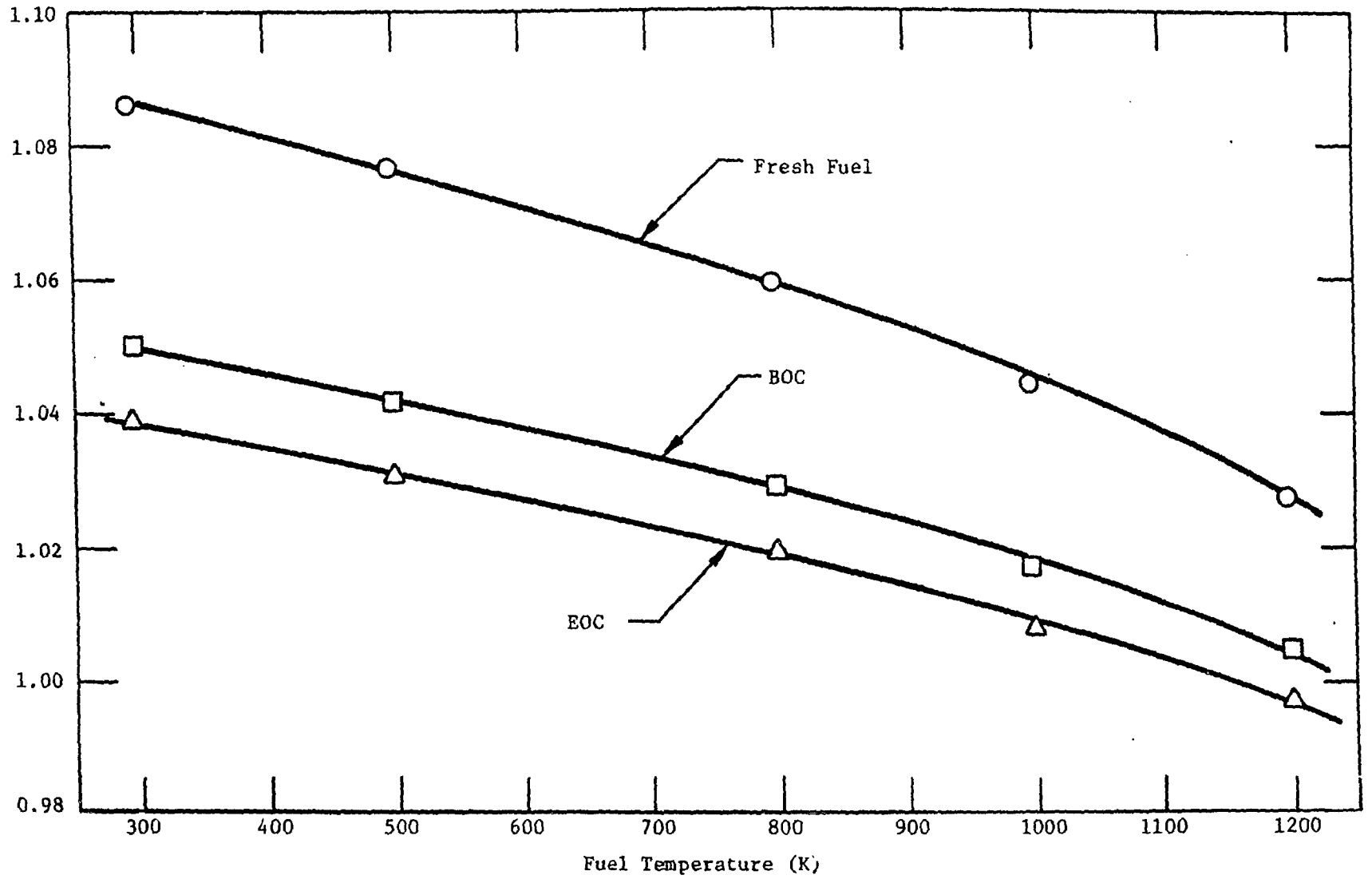

Fig. 9. k_{eff} as a function of fuel temperature for fresh fuel, BOC, and EOC cores.

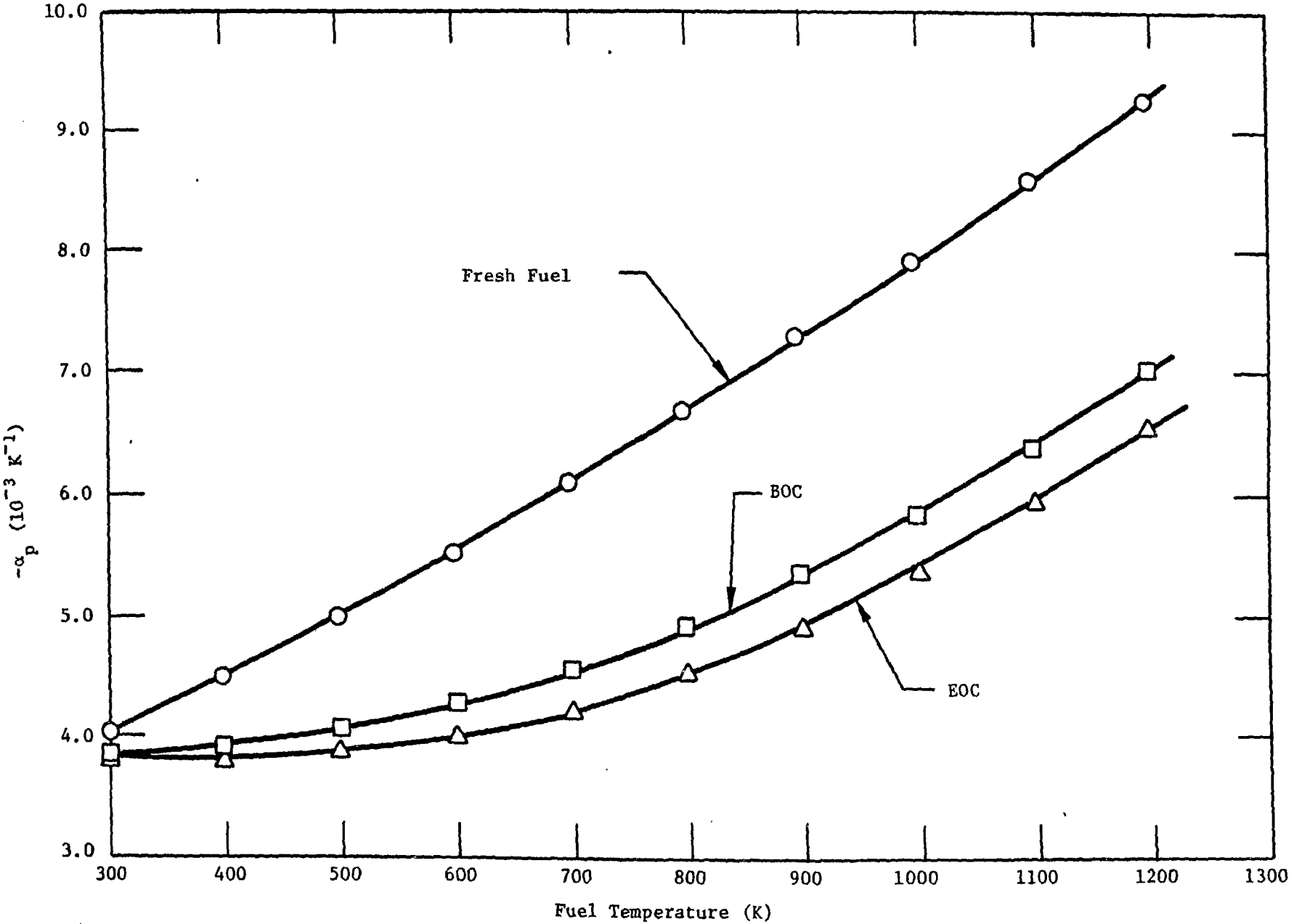

Fig. 10. Prompt negative temperature coefficient as a function of temperature for fresh fuel, BOC, and EOC cores.

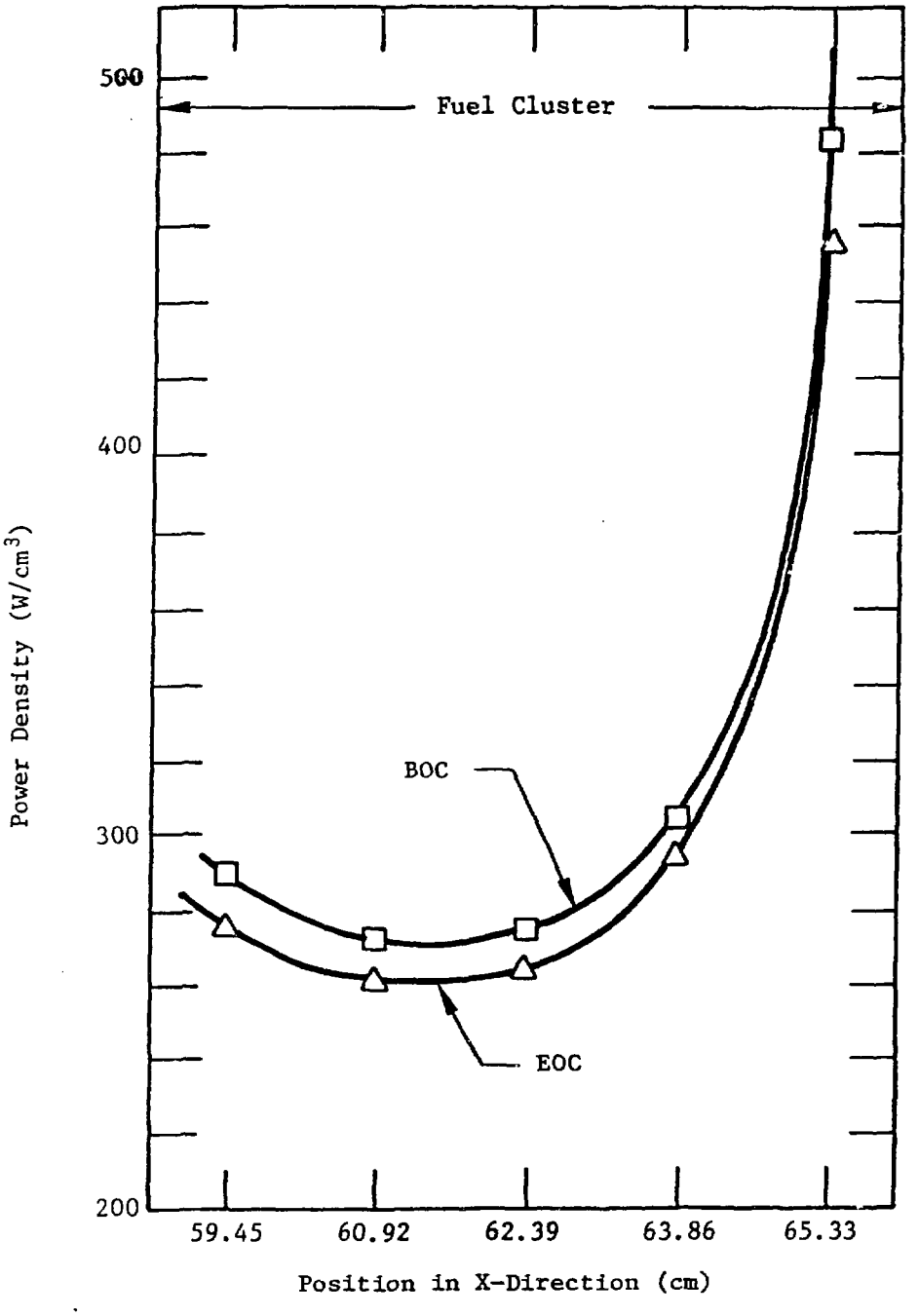

Fig. 11a. Power profile in X-direction through element FE9G which contains the core hot spot.

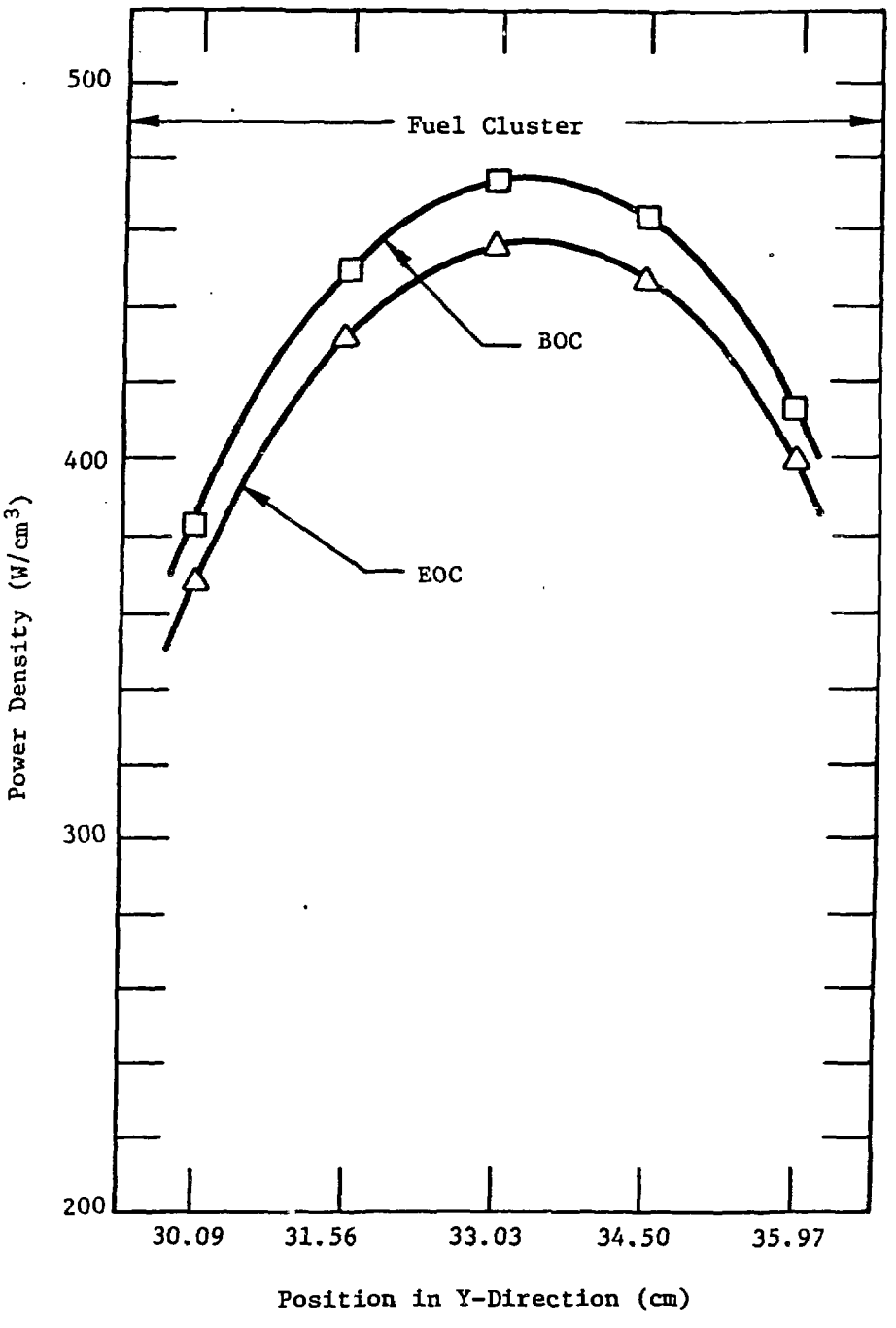

Fig. 11b. Power profile in Y-direction through element FE9G which contains the core hot spot.